# Visualizing fast growth of large single-crystalline graphene by tunable isotopic carbon source

Luzhao Sun<sup>1,2,§</sup>, Li Lin<sup>1,§</sup>, Jincan Zhang<sup>1,2</sup>, Huan Wang<sup>1</sup>, Hailin Peng<sup>1</sup> (🖂), and Zhongfan Liu<sup>1</sup> (🖂)

Received: 27 July 2016 Revised: 1 September 2016 Accepted: 23 September 2016

© Tsinghua University Press and Springer-Verlag Berlin Heidelberg 2016

## **KEYWORDS**

large single-crystalline graphene, fast growth, isotope labelling, carbon source

#### **ABSTRACT**

The fast growth of large single-crystalline graphene by chemical vapor deposition on Cu foil remains a challenge for industrial-scale applications. To achieve the fast growth of large single-crystalline graphene, understanding the detailed dynamics governing the entire growth process—including nucleation, growth, and coalescence—is important; however, these remain unexplored. In this study, by using a pulsed carbon isotope labeling technique in conjunction with micro-Raman spectroscopy identification, we visualized the growth dynamics, such as nucleation, growth, and coalescence, during the fast growth of large single-crystalline graphene domains. By tuning the supply of the carbon source, a growth rate of 320  $\mu m/min$  and the growth of centimeter-sized graphene single crystals were achieved on Cu foil.

#### 1 Introduction

Graphene is an emerging material for applications in various electronics and optoelectronics owing to its unique structural, electrical, and optical properties [1–4]. The production of large-area, high-quality, single-crystalline graphene film, which is required for the practical realization of electronic-grade graphene-based technology, is perhaps one of the most challenging tasks and is in its infancy [5, 6]. Among the synthetic methods enabling the production of graphene, chemical

vapor deposition (CVD) employing transition metals—especially Cu foil—hold great promise with regard to the growth of large-area graphene films with a domain quality comparable to that of mechanically exfoliated graphene [6–12]. For instance, through the introduction of oxygen, the careful pretreatment of the substrate, and a low precursor supply, centimeter-scale graphene single crystals can be successfully grown; however, these are usually achieved with a low growth rate of few micrometers per minute [5, 6, 13]. The long growth time of several hours leads to a high

Address correspondence to Zhongfan Liu, zfliu@pku.edu.cn; Hailin Peng, hlpeng@pku.edu.cn



<sup>&</sup>lt;sup>1</sup> Center for Nanochemistry, Beijing Science and Engineering Center for Nanocarbons, Beijing National Laboratory for Molecular Sciences, College of Chemistry and Molecular Engineering, Peking University, Beijing 100871, China

<sup>&</sup>lt;sup>2</sup> Academy for Advanced Interdisciplinary Studies, Peking University, Beijing 100871, China

<sup>§</sup> These authors contributed equally to this work.

energy-consumption during the high-temperature CVD process for graphene crystals. Thus, a major hurdle remains for achieving the fast and controllable growth of large single-crystalline graphene: improving the output quality and energy consumption [14–16].

For the realization of the rapid growth of large single-crystalline graphene, a full understating of the growth dynamics, including nucleation, growth, and coalescence of single domains, is needed to enable rational process optimization [17]. However, the detailed growth dynamics during the fast growth of large single-crystalline graphene remains largely unexplored [18–20]. There have been several reports regarding the in situ observation of graphene growth via environmental scanning electron microscopy [21, 22] or radiation-mode optical microscopy (OM) [23]; however, the growth behavior of large graphene single crystals has not been reported. Fortunately, the evolution of graphene domains is driven by the lateral attachment of carbon atoms onto the edges of the graphene basal plane, which can be labeled with carbon isotopes for visualizing growth process of graphene in conjunction with ex situ Raman spectroscopy [24]. The carbon isotope labeling technique was demonstrated for investigating the formation mechanism, diffusion mechanism, and stacking orientation of graphene grown on Cu foil [5, 10, 24–28]. Nevertheless, such routines mainly rely on the switch between normal methane (12CH<sub>4</sub>) and 13C-labeled methane (13CH<sub>4</sub>), which might produce unavoidable perturbation of the growth during carbon-source switching, especially when an extremely low supply of carbon source is utilized for the suppression of nucleation during the rapid growth of a large graphene domain. In particular, new domain nuclei might emerge during the switching (Fig. S1 in the Electronic Supplementary Material (ESM)).

In this study, we visualized the nucleation and fast growth of large single-crystalline graphene by using the isotopic pulse-labeling technique; i.e., <sup>12</sup>CH<sub>4</sub> was continuously present in the chamber during the entire growth period and was kept unchanged while pulses of a small amount of <sup>13</sup>CH<sub>4</sub> were sequentially introduced with minimum perturbation (Fig. S2 in the ESM). The time evolution of the growth of large single-crystalline graphene is clearly presented in

conjunction with the Raman maps, which can fingerprint the corresponding growth dynamic, especially regarding the roles of the carbon source in the control of the nucleation and growth. Importantly, based on such investigation, the growth of centimeter-sized graphene single crystals and a growth rate of 320 µm/min for growing millimeter-sized graphene single crystals are realized by carefully tuning the carbon source, which are highly important for achieving the energy-efficient growth of high-quality graphene for further applications. Deep insights regarding the influence of the carbon source on the growth dynamics of the nucleation and the final coalescence are also presented.

#### Results and discussion

Figure 1(a) shows a schematic of the CVD growth of <sup>13</sup>C-pulse-labeled large single-crystalline graphene and the visualization of the temporal evolution using Raman spectroscopy. The Cu foil was exposed to <sup>12</sup>CH<sub>4</sub> at constant fluxes, and a small amount of <sup>13</sup>CH<sub>4</sub> pulses was introduced in a specific sequence (Fig. S3 in the ESM). Owing to the surface-mediated growth mechanism of graphene on Cu and the separated Raman modes of <sup>12</sup>C and <sup>13</sup>C, the visualization of the spatial distribution of isotopic carbon atoms and the corresponding growth dynamics of graphene becomes feasible [24]. There are two characteristic Raman modes of <sup>12</sup>C-composed graphene: the G peak at ~1,580 cm<sup>-1</sup>  $(G^{12})$  and the 2D peak at ~2,690 cm<sup>-1</sup> (2D<sup>12</sup>). The corresponding area grown with <sup>13</sup>CH<sub>4</sub> pulses, which contains 12C-12C, 12C-13C, and 13C-13C bonds, decreases the G peak to  $1580 \times [12/(12 + \alpha)]^{1/2}$  cm<sup>-1</sup> (G<sup>12+13</sup>) and the 2D peak to  $2690 \times [12/(12 + \alpha)]^{1/2}$  cm<sup>-1</sup> (2D<sup>12+13</sup>), where  $\alpha$  is the percentage of <sup>13</sup>C (Fig. S4 in the ESM) [29, 30].

The as-grown centimeter-sized graphene domains labeled with the sequential introduction of <sup>13</sup>CH<sub>4</sub>-pulses all exhibit a rectangular shape (Fig. 1(b)) owing to the identical orientations of the underlying Cu(100) substrate, as confirmed in a recent work [31]. A detailed discussion regarding the structure of square graphene domains is presented in Fig. S5 in the ESM. To investigate the corresponding time evolution and growth rate precisely, Raman mapping was conducted for graphene transferred onto a Si/SiO<sub>2</sub> substrate

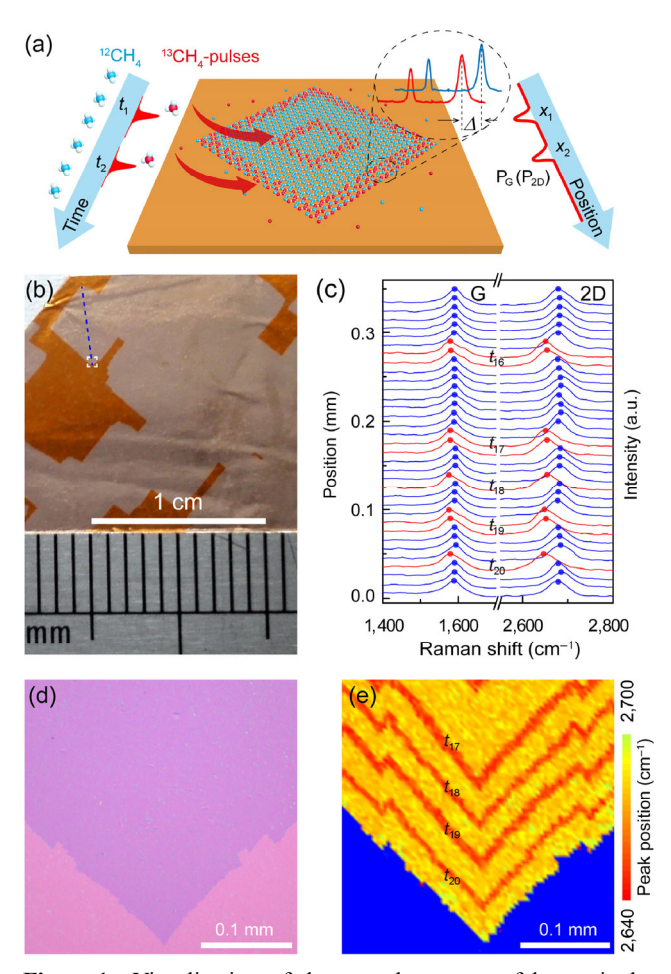
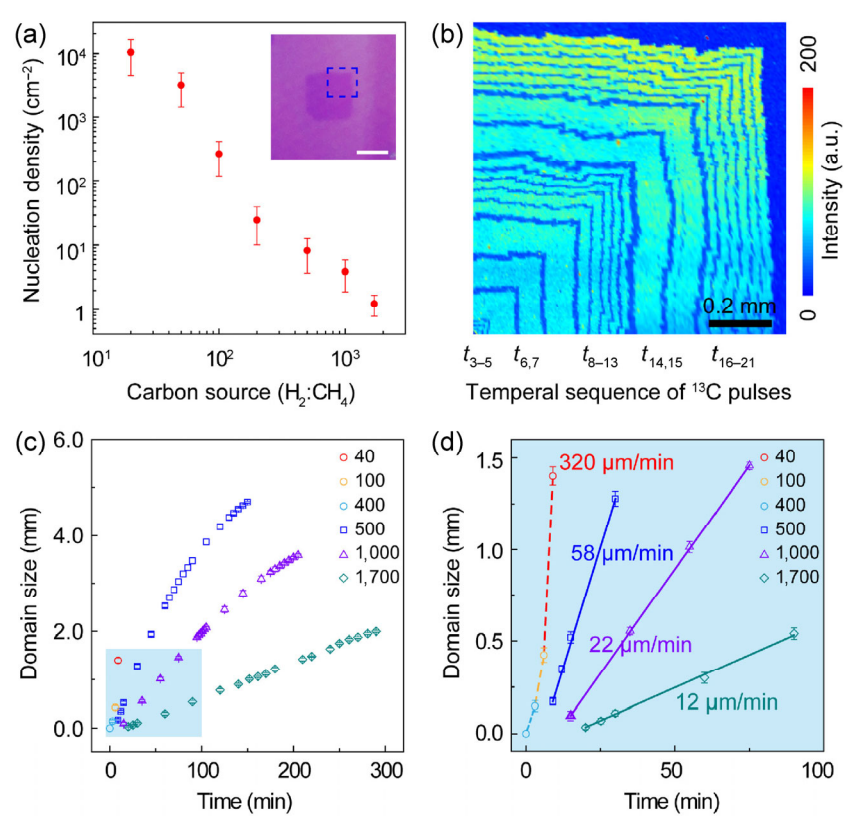


Figure 1 Visualization of the growth process of large singlecrystal graphene on a Cu surface by the isotopic pulse-labelling technique in conjunction with micro-Raman spectroscopy. (a) Schematic of the pulsed carbon isotope labeling process and the separated Raman mode of <sup>12</sup>C and <sup>13</sup>C in the graphene basal plane. The red and blue balls represent <sup>13</sup>C and <sup>12</sup>C atoms, respectively. The Cu surface is exposed to a constant flux of <sup>12</sup>CH<sub>4</sub> along with the sequential introduction of <sup>13</sup>CH<sub>4</sub> pulses. The distribution of the pulsed carbon isotope is reflected by utilizing the separated Raman modes of  ${}^{12}$ C and  ${}^{13}$ C in the graphene basal plane.  $t_i$  (i =1, 2, ...) represents the temporal sequence of introducing <sup>13</sup>CH<sub>4</sub> pulses, while  $x_i$  (i = 1, 2, ...) indicates the responding distribution position of pulsed <sup>13</sup>C in the as-grown graphene basal plane. (b) Photograph of centimeter-sized graphene domains grown on the Cu foil. (c) Series of Raman spectra recorded along the diagonal of the graphene domain marked in (b), corresponding to the <sup>13</sup>C pulses from  $t_{16}$  to  $t_{20}$  during the graphene growth (see Fig. S3 in the ESM). (d) and (e) OM image of large single-crystalline graphene in (b) transferred onto a SiO<sub>2</sub>/Si substrate (d) and the corresponding Raman 2D-band position map (e).

(Figs. 1(c) and 1(d)). The line scan of Raman spectra along the diagonal of the graphene domain displays a clear shift in the G peaks and 2D peaks toward a lower wavenumber, indicating the presence of an isotope-engineered region (Fig. 1(c) and Fig. S6 in the ESM). The Raman 2D-band position map (Fig. 1(e)) clearly shows the spatial distribution of isotopic carbon atoms, in which the red strips (2D peaks here are around 2,645 cm<sup>-1</sup>) represent the temporal sequence of the introduction of  $^{13}$ CH<sub>4</sub> pulses (marked as time  $t_i$ , i = 1, 2, 3, ...). In conjunction with the spatial distribution of the carbon isotopes (marked as position  $x_i$ , i = 1, 2, 3, ...), the time-dependent growth behavior can thus be visualized. By investigating the growth behavior though the tuning and labeling of the carbon-source supplies, the corresponding growth rate and growth dynamics are unveiled.

The CVD growth of graphene on Cu foil can be simplified into the following elemental procedures: 1) the decomposition of the carbon source at the active sites of the Cu surface, 2) the subsequent nucleation, 3) further growth, and 4) the coalescence of graphene domains toward continuous films [9, 17, 32]. The active carbon species provided by the decomposition of the carbon source fuels both the nucleation and the epitaxial growth of graphene. In such a case, the amount of active carbon species produced on the Cu surface, which can be intentionally tuned by changing the carbon-source supply, determines the nucleation density and growth rate of graphene. In our experiment, the hydrogen-to-methane ratio (H<sub>2</sub>:CH<sub>4</sub>) is tuned to control the relative carbon-source supply for the investigation of the influence of these substances on the graphene growth [6, 33]. For instance, the flux of methane is constantly kept as 1 standard-state cubic centimeter per minute (sccm), and that of hydrogen is tuned from 20 to 1,700 sccm (Fig. 2(a)). The corresponding plot shows a clear suppression of the nucleation density due to a decrease in the supply of the carbon source (Fig. 2(a) and Fig. S7 in the ESM), which results in the formation of sub centimeter-sized graphene domains. For instance, a square graphene domain with area of ~2 mm<sup>2</sup> (inset of Fig. 2(a)) was successfully grown with  $H_2:CH_4 = 1,700$  (nucleation density  $\sim 1.2$  cm<sup>-2</sup>, Fig. S7(a) in the ESM).

To better visualize the time-dependent growth rate of the domains in the early stage (nucleation stage), intermediate stage (further growth), and final stage (coalescence stage) of the growth process, the isotopic



**Figure 2** Influence of the carbon source on the nucleation density and growth rate of large single-crystalline graphene. (a) Nucleation density of graphene as a function of the carbon source. Inset: an OM image of typical graphene on a SiO<sub>2</sub>/Si substrate with a low nucleation density. The scale bar represents 1 mm. (b) Raman 2D<sup>12</sup>-band intensity map of the area marked in the inset of (a). (c) Domain size (diagonal of graphene domains) of as-grown large single-crystalline graphene as a function of the growth time. The H<sub>2</sub>:CH<sub>4</sub> ratio ranges from 40 to 1,700. (d) Magnification of the early stage of graphene growth shadowed in (c). A growth rate of 320 μm/min was realized by the gradual increase of the carbon-source supply (for detailed growth parameters, please see the ESM).

pulses are intensively introduced, and the corresponding Raman characterization and analysis are performed. For instance, the 2D<sup>12</sup>-band intensity map of a quarter of the square graphene domain enclosed in the dashed-line box in the inset of Fig. 2(a) is presented in Fig. 2(b), from which the domain sizes as functions of growth time can be extracted (the dark cyan data points in Fig. 2(c)).

The domain sizes increase linearly with the growth time at the early stage of graphene growth (Fig. 2(d)), probably owing to the sufficiently uncovered catalytic Cu surface. As previously discussed, in such a case, the growth rate is mainly determined by the carbon-source supply, where a high carbon-source supply (i.e., low H<sub>2</sub>:CH<sub>4</sub>) yields faster growth. The growth rate becomes saturated when the coverage of graphene domains on the Cu foil reaches a certain level [34]. The corresponding coverage profiles exhibit a similar

saturation tendency, which is presumably caused by the gradual reduction in the active catalytic area of the Cu foil (Fig. S8 in the ESM) [22, 34]. Clearly, a sufficient carbon-source supply promotes a faster growth stage, thereby realizing less time consumed in the formation of a continuous film.

The carbon-source supply determines the quality and energy consumption of CVD-grown graphene [6, 33]. In this regard, a stepwise increase in the carbon-source supply before the saturation point was conducted to achieve a high growth rate without significantly degrading the domain sizes. Clearly, by the intentional control of the carbon-source supply (Figs. S9 and S10 in the ESM), the growth rate can reach ~320  $\mu$ m/min, which is among the best results for the growth of millimeter-sized single-crystalline graphene domains. It is well established that the active carbon species prefers to stick to the already existing

graphene nuclei rather than form new nuclei [18, 19, 33]. Thus, if the carbon-source supply increases slightly, the enhanced as-produced carbon species is more likely to contribute to the epitaxial growth of the original nuclei, with only a few new nucleation appearing. Of course, if the carbon-source supply is increased significantly, spontaneous nucleation cannot be avoided [35]. Thus, based on the investigation of the correlation between the carbon source and the growth rate, a tradeoff between the domain size and the growth rate in the mass production of large single-crystalline graphene can be achieved by intentionally designing the carbon-source supply in an energy-saving manner.

We studied the significant role of the carbon-source supply during the nucleation stage (Fig. 3). Figure 3(a) shows graphene nuclei grown for 5 min that exhibit different domain sizes. Interestingly, as shown in the corresponding Raman maps and the schematic of the isotopic distribution (Figs. 3(b) and 3(c)), the marker of the first <sup>13</sup>C pulse (at 0.5 min) is missing, and

graphene is nucleated during the interval between the second and third pulses, indicating that additional time (the nucleation time) was necessary for graphene nucleation. In this regard, the nucleation time for each grain can be inferred from the plots of the domain size as a function of the growth time (Figs. S11 and S12 in the ESM) and is summarized in Fig. 3(d). At microscopic scales, the nucleation is not completed within a very short period of time, because the active carbon species must overcome a certain energy barrier to form carbon clusters and subsequently nuclei. Such an energy barrier is related to the catalytic ability of the underlying substrate, which differs depending on location, leading to a variation in the nucleation time, even under the same growth conditions [18, 19, 33]. The energy barrier is overcome by forming a stable cluster with the critical size through the collision among the active carbon species. Consequently, the probability of overcoming the nucleation barrier is related to the collision rate among the carbon species produced on the Cu surface, which can be tuned by

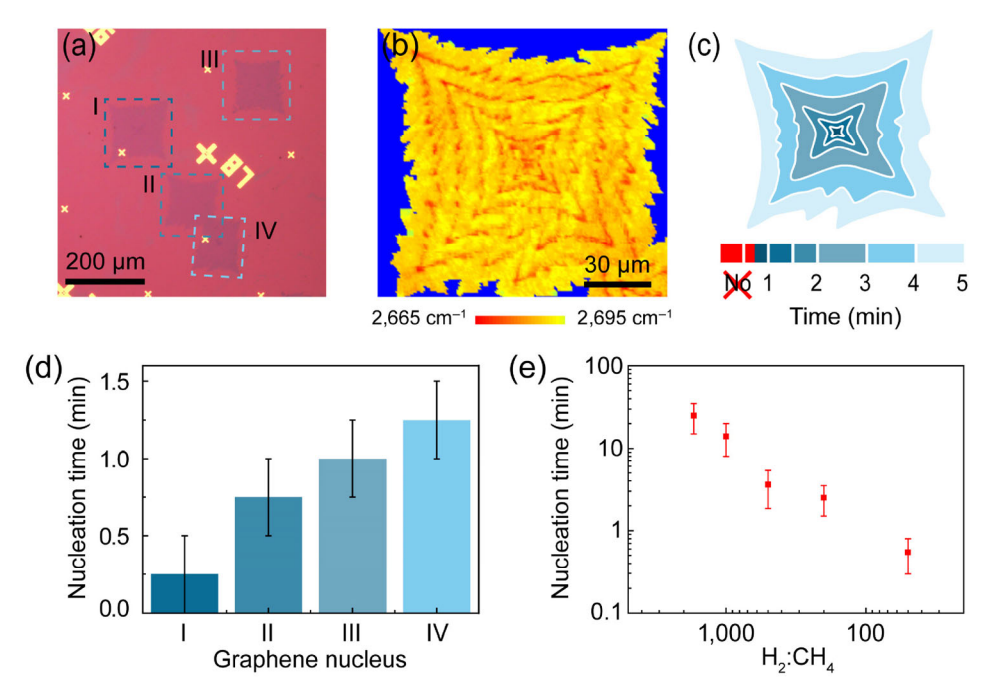


**Figure 3** Nucleation time of large single-crystalline graphene. (a) OM image of graphene nuclei on a SiO<sub>2</sub>/Si substrate. (b) Raman 2D-band position map (2,665–2,695 cm<sup>-1</sup>) corresponding to nucleus II in (a). The blue color denotes the SiO<sub>2</sub> substrate. (c) Schematic of the isotopic distribution and corresponding growth sequences of the graphene nucleus in (b). The white strokes denote the presence of <sup>13</sup>C pulses, and the intervals between <sup>13</sup>C pulses are colored with different shades of blue to clarify the introduction sequence of the <sup>13</sup>C pulses. The red area indicates the missed <sup>13</sup>C pulses and inferred nucleation time. (d) Nucleation time of the graphene nuclei in (a). (e) Nucleation time as a function of the H<sub>2</sub>:CH<sub>4</sub> ratio. The error bars are from calculations of different domains for each growth condition.

changing the carbon-source supply. A higher carbon-source supply increases the collision rate among active carbon atoms, which may help to overcome the barrier, form nuclei, and thus reduce the nucleation time (Fig. 3(e)). In our experiment, the etching effect of hydrogen is dominant when the H<sub>2</sub>:CH<sub>4</sub> content is high, which makes it difficult for graphene clusters to grow to the critical size, leading to a long nucleation time.

For the growth of large single-crystalline graphene, a difference in the nucleation time results in a wide distribution of the domain size of the as-grown graphene and a non-uniformity in the overall quality of the as-synthesized films. Thus, tuning the carbon source properly and providing a flat surface to reduce the differences in the nucleation behavior are promising methods for further enhancing the uniformity of the graphene film.

In addition to large single-crystalline graphene domains, a continuous graphene film caused by the coalescence of individual domains is required for industrial-scale applications. However, the coalescence

region might suffer from a gradual reduction in the active Cu area to catalyze the carbon source to fuel the growth at the frontier during the merging process (between domains I and II in Fig. 4(a)). This may result in a reduced growth rate and even the incapability of merging each grain [25]. In contrast, another edge of domain II was constantly surrounded by a sufficient amount of active Cu during growth. This difference may lead to different growth rates if the as-formed active carbon species are supposed to be catalyzed by the active Cu and diffuse toward the growth frontier for the growth of graphene. However, the difference in the growth of the two frontiers is confirmed to be nearly zero (Fig. 4(b)), indicating the existence of another channel through which the carbon source participates in the growth. In addition, a saturated growth rate exists at both growth frontiers, demonstrating that the growth rate depends on the coverage of graphene over the whole Cu foil rather than in the active Cu region nearby (inset of Fig. 4(b)). Consequently, the active carbon species are shared among all domains owing to the presence of an additional channel; active

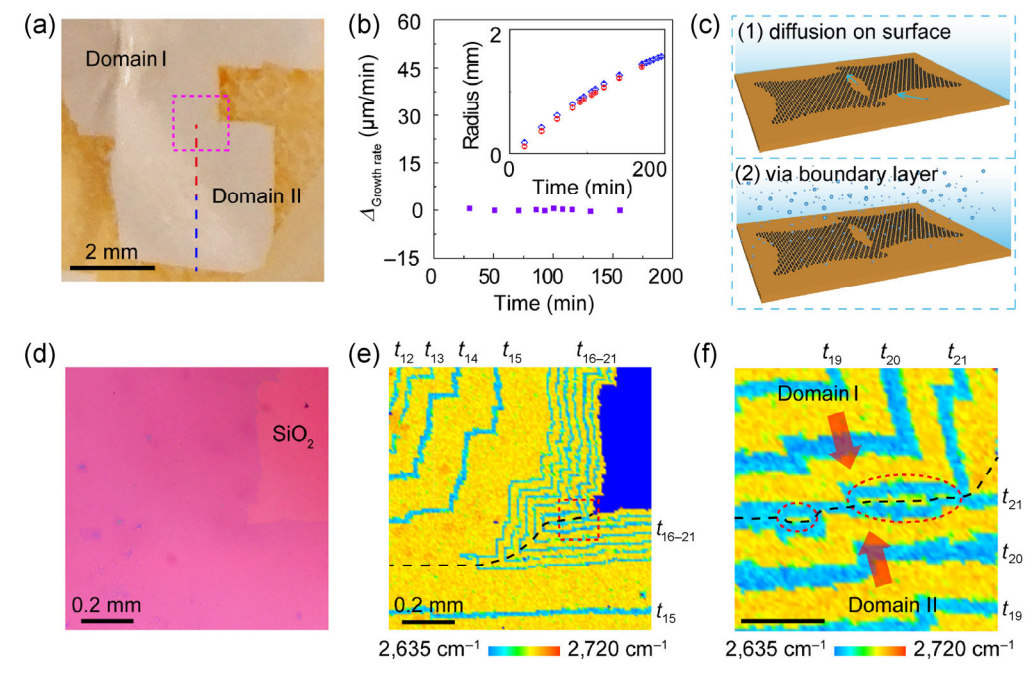


Figure 4 Coalescence of large single-crystalline graphene domains. (a) Photograph of the merging region between graphene domains on Cu foil. (b) Difference of the calculated growth rates along the two directions of the graphene grains marked in (a). Inset: the corresponding domain size (radius) as a function of the growth time along the two directions. (c) Two possible channels through which active carbon species can participate in the graphene growth: (1) on-surface diffusion, and (2) transportation through the boundary layer. (d) and (e) OM image (d) and corresponding Raman 2D-band position map (e) of the merging region marked in (b). (f) High-magnification Raman map of the region marked in (d). The scale bar represents 50 μm.

carbon species in the boundary layer near the Cu surface (Fig. 4(c)), which are produced from the entire Cu surface, assist with the growth of graphene and the formation of a continuous film [9].

Figures 4(d)–4(f) show the detailed time evolution of the coalescence between the two domains (for the temporal sequence, see the ESM). The region marked in Fig. 4(f) is formed after the last pulse, indicating that this region is uncovered when the surrounding Cu is covered by graphene (uncovered Cu islands). Consequently, the active carbon species participating in the formation of such a region are supplied by another channel rather than produced by the limited active Cu nearby. Importantly, such a transport channel at the boundary layer may result in the fast coalescence of the domains. In addition, the <sup>13</sup>C-pulse-labeled CVD method, along with the Raman maps, provides the opportunity to visualize the presence and temporal evolution of the boundaries (Fig. 4(e)) [36].

#### 3 Conclusions

We visualized the growth dynamics for the fast growth of large single-crystalline graphene, including the nucleation, growth, and coalescence stages, using a carbon isotopic pulse-labeling technique in conjunction with Raman spectroscopy. A fast growth rate of 320  $\mu$ m/min, which is among the best results for the growth of millimeter-sized graphene crystals, was realized by tuning the carbon source. This work provides new insights into the mechanism of graphene growth and is a significant step toward the growth of high-quality graphene crystals in an energy-efficient manner for industrial applications.

#### 4 Method

## 4.1 Graphene growth

Graphene is synthesized in a low-pressure CVD system with a system pressure no greater than 2 kPa. Commercially available Cu foil (98% purity, 25 µm thick, Alfa-Aesar #46365) is vertically stacked and placed in the hot center of a furnace (Lindberg/Blue M) after being electrochemically polished for 30 min at an electrical current density ranging from 75 to 500 A/m².

The polishing solution is composed of phosphoric acid and ethylene glycol, with a volume ratio of 3:1. Subsequently, the system is heated to 1,020 °C under an Ar flow of 500 sccm, with a pressure of 480 Pa. After a temperature of 1,020 °C is reached, the Cu foil is annealed with no reducing gas and 500 sccm H<sub>2</sub> (~480 Pa) for 10 and 5 min, respectively. The no-gas annealing introduces a small amount of oxygen, which promotes the monocrystallization of the Cu foil [31] and passivates the nucleation sites, reducing the nucleation density. Subsequently, the growth of graphene is initiated by introducing CH<sub>4</sub> and H<sub>2</sub>. The H<sub>2</sub>:CH<sub>4</sub> ratio is carefully selected to control the carbon source for the enhancement of the growth rate and the suppression of spontaneous nucleation.

#### 4.2 Graphene transfer

The graphene is transferred onto a SiO<sub>2</sub>/Si (with 280-nm-thick SiO<sub>2</sub>) substrate with the assistance of poly methyl methacrylate (PMMA). The graphene grown on the Cu foil is spin-coated with PMMA at 2,000 rpm (revolutions per minute) 2 kr/min and then baked at 170 °C for 5 min. The as-formed sandwich structure of PMMA/graphene/Cu is placed and floated on the surface of an FeCl<sub>3</sub> (1 mol/L) etching solution after the graphene on the other side of the Cu is removed by being exposed to air plasma for 5 min with a flux of 15 sccm and a power of 90 W. Subsequently, after the etching of the Cu, the freestanding PMMA/ graphene film floating on the etching solution is washed thoroughly with deionized water 3-5 times. Then, the film is salvaged by the SiO<sub>2</sub>/Si substrate. The formed structure of PMMA/graphene/SiO<sub>2</sub>/Si is then dried, followed by immersion in acetone at 100 °C, which dissolves the PMMA and reveals the graphene on the target substrate.

### 4.3 Characterization

The graphene domains on the Cu foil are heated in air at 170 °C for 10 min to oxidize the bare Cu and make them visible. The visible graphene domains on Cu and SiO<sub>2</sub>/Si are characterized using an optical microscope (Olympus BX51) and a Raman spectrometer (Horiba, LabRAM HR-800, ×100 objective and wavelength of 514 nm).

## Acknowledgements

This work was financially supported by the National Basic Research Program of China (Nos. 2013CB932603, 2012CB933404 and 2014CB932500), the National Natural Science Foundation of China (Nos. 51432002, 51520105003, and 21525310), National Program for Support of Top-Notch Young Professionals, and Beijing Municipal Science & Technology Commission (No. Z161100002116002).

**Electronic Supplementary Material**: Supplementary material (detailed experimental section, schematic of the fabrication process, Raman spectroscopy measurements, TEM image and so on) is available in the online version of this article at http://dx.doi.org/10.1007/s12274-016-1297-1.

#### References

- [1] Novoselov, K. S.; Geim, A. K. The rise of graphene. *Nat. Mater.* **2007**, *6*, 183–191.
- [2] Zhang, Y. B.; Tan, Y. W.; Stormer, H. L.; Kim, P. Experimental observation of the quantum hall effect and berry's phase in graphene. *Nature* 2005, 438, 201–204.
- [3] Bonaccorso, F.; Sun, Z.; Hasan, T.; Ferrari, A. C. Graphene photonics and optoelectronics. *Nat. Photonics* 2010, 4, 611–622.
- [4] Huang, X.; Zeng, Z. Y.; Fan, Z. X.; Liu, J. Q.; Zhang, H. Graphene-based electrodes. Adv. Mater. 2012, 24, 5979–6004.
- [5] Hao, Y. F.; Bharathi, M. S.; Wang, L.; Liu, Y. Y.; Chen, H.; Nie, S.; Wang, X. H.; Chou, H.; Tan, C.; Fallahazad, B. et al. The role of surface oxygen in the growth of large singlecrystal graphene on copper. *Science* 2013, 342, 720–723.
- [6] Zhou, H. L.; Yu, W. J.; Liu, L. X.; Cheng, R.; Chen, Y.; Huang, X. Q.; Liu, Y.; Wang, Y.; Huang, Y.; Duan, X. F. Chemical vapour deposition growth of large single crystals of monolayer and bilayer graphene. *Nat. Commun.* 2013, 4, 2096.
- [7] Reina, A.; Jia, X. T.; Ho, J.; Nezich, D.; Son, H.; Bulovic, V.; Dresselhaus, M. S.; Kong, J. Large area, few-layer graphene films on arbitrary substrates by chemical vapor deposition. *Nano Lett.* 2009, 9, 30–35.
- [8] Li, X. S.; Cai, W. W.; An, J. H.; Kim, S.; Nah, J.; Yang, D. X.; Piner, R.; Velamakanni, A.; Jung, I.; Tutuc, E. et al. Large-area synthesis of high-quality and uniform graphene films on copper foils. *Science* 2009, 324, 1312–1314.
- [9] Bhaviripudi, S.; Jia, X. T.; Dresselhaus, M. S.; Kong, J.

- Role of kinetic factors in chemical vapor deposition synthesis of uniform large area graphene using copper catalyst. *Nano Lett.* **2010**, *10*, 4128–4133.
- [10] Li, X. S.; Magnuson, C. W.; Venugopal, A.; Tromp, R. M.; Hannon, J. B.; Vogel, E. M.; Colombo, L.; Ruoff, R. S. Large-area graphene single crystals grown by low-pressure chemical vapor deposition of methane on copper. *J. Am. Chem. Soc.* 2011, 133, 2816–2819.
- [11] Yan, Z.; Lin, J.; Peng, Z. W.; Sun, Z. Z.; Zhu, Y.; Li, L.; Xiang, C. S.; Samuel, E. L.; Kittrell, C.; Tour, J. M. Toward the synthesis of wafer-scale single-crystal graphene on copper foils. *ACS Nano* **2012**, *6*, 9110–9117.
- [12] Reina, A.; Thiele, S.; Jia, X. T.; Bhaviripudi, S.; Dresselhaus, M. S.; Schaefer, J. A.; Kong, J. Growth of large-area single-and bi-layer graphene by controlled carbon precipitation on polycrystalline Ni surfaces. *Nano Res.* 2009, 2, 509–516.
- [13] Lin, L.; Li, J. Y.; Ren, H. Y.; Koh, A. L.; Kang, N.; Peng, H. L.; Xu, H. Q.; Liu, Z. F. Surface engineering of copper foils for growing centimeter-sized single-crystalline graphene. ACS Nano 2016, 10, 2922–2929.
- [14] Geng, D. C.; Wang, H. P.; Yu, G. Graphene single crystals: Size and morphology engineering. *Adv. Mater.* **2015**, *27*, 2821–2837.
- [15] Li, X. S.; Colombo, L.; Ruoff, R. S. Synthesis of graphene films on copper foils by chemical vapor deposition. *Adv. Mater.* **2016**, *28*, 6247–6252.
- [16] Wu, T. R.; Zhang, X. F.; Yuan, Q. H.; Xue, J. C.; Lu, G. Y.; Liu, Z. H.; Wang, H. S.; Wang, H. M.; Ding, F.; Yu, Q. K. et al. Fast growth of inch-sized single-crystalline graphene from a controlled single nucleus on Cu-Ni alloys. *Nat. Mater.* 2016, 15, 43–48.
- [17] Yan, K.; Fu, L.; Peng, H. L.; Liu, Z. F. Designed CVD growth of graphene via process engineering. *Acc. Chem. Res.* **2013**, 46, 2263–2274.
- [18] Gao, J. F.; Yip, J.; Zhao, J. J.; Yakobson, B. I.; Ding, F. Graphene nucleation on transition metal surface: Structure transformation and role of the metal step edge. *J. Am. Chem. Soc.* 2011, 133, 5009–5015.
- [19] Yuan, Q. H.; Gao, J. F.; Shu, H. B.; Zhao, J. J.; Chen, X. S.; Ding, F. Magic carbon clusters in the chemical vapor deposition growth of graphene. J. Am. Chem. Soc. 2012, 134, 2970–2975.
- [20] Zhang, X. Y.; Wang, L.; Xin, J.; Yakobson, B. I.; Ding, F. Role of hydrogen in graphene chemical vapor deposition growth on a copper surface. *J. Am. Chem. Soc.* 2014, 136, 3040–3047.
- [21] Kidambi, P. R.; Bayer, B. C.; Blume, R.; Wang, Z. J.; Baehtz, C.; Weatherup, R. S.; Willinger, M. G.; Schloegl, R.; Hofmann, S. Observing graphene grow: Catalyst–graphene

- interactions during scalable graphene growth on polycrystalline copper. *Nano Lett.* **2013**, *13*, 4769–4778.
- [22] Wang, Z. J.; Weinberg, G.; Zhang, Q.; Lunkenbein, T.; Klein-Hoffmann, A.; Kurnatowska, M.; Plodinec, M.; Li, Q.; Chi, L. F.; Schloegl, R. et al. Direct observation of graphene growth and associated copper substrate dynamics by *in situ* scanning electron microscopy. *ACS Nano* 2015, 9, 1506–1519.
- [23] Terasawa, T. O.; Saiki, K. Radiation-mode optical microscopy on the growth of graphene. *Nat. Commun.* **2015**, *6*, 6834.
- [24] Li, X. S.; Cai, W. W.; Colombo, L.; Ruoff, R. S. Evolution of graphene growth on Ni and Cu by carbon isotope labeling. *Nano Lett.* **2009**, *9*, 4268–4272.
- [25] Li, X. S.; Magnuson, C. W.; Venugopal, A.; An, J. H.; Suk, J. W.; Han, B. Y.; Borysiak, M.; Cai, W. W.; Velamakanni, A.; Zhu, Y. W. et al. Graphene films with large domain size by a two-step chemical vapor deposition process. *Nano Lett.* 2010, 10, 4328–4334.
- [26] Fang, W. J.; Hsu, A. L.; Caudillo, R.; Song, Y.; Birdwell, A. G.; Zakar, E.; Kalbac, M.; Dubey, M.; Palacios, T.; Dresselhaus, M. S. et al. Rapid identification of stacking orientation in isotopically labeled chemical-vapor grown bilayer graphene by Raman spectroscopy. *Nano Lett.* 2013, 13, 1541–1548.
- [27] Li, Q. Y.; Chou, H.; Zhong, J. H.; Liu, J. Y.; Dolocan, A.; Zhang, J. Y.; Zhou, Y. H.; Ruoff, R. S.; Chen, S. S.; Cai, W. W. Growth of adlayer graphene on Cu studied by carbon isotope labeling. *Nano Lett.* 2013, *13*, 486–490.
- [28] Zhao, Z. J.; Shan, Z. F.; Zhang, C. K.; Li, Q. Y.; Tian, B.; Huang, Z. Y.; Lin, W. Y.; Chen, X. P.; Ji, H. X.; Zhang, W. F. et al. Study on the diffusion mechanism of graphene grown on copper pockets. *Small* 2015, 11, 1418–1422.
- [29] Cai, W. W.; Piner, R. D.; Stadermann, F. J.; Park, S.; Shaibat, M. A.; Ishii, Y.; Yang, D. X.; Velamakanni, A.; An, S. J.;

- Stoller, M. et al. Synthesis and solid-state NMR structural characterization of <sup>13</sup>C-labeled graphite oxide. *Science* **2008**, *321*, 1815–1817.
- [30] Carvalho, B. R.; Hao, Y. F.; Righi, A.; Rodriguez-Nieva, J. F.; Colombo, L.; Ruoff, R. S.; Pimenta, M. A.; Fantini, C. Probing carbon isotope effects on the Raman spectra of graphene with different <sup>13</sup>C concentrations. *Phys. Rev. B* 2015, 92, 125406.
- [31] Wang, H.; Xu, X. Z.; Li, J. Y.; Lin, L.; Sun, L. Z.; Sun, X.; Zhao, S. L.; Tan, C. W.; Chen, C.; Dang, W. H. et al. Surface monocrystallization of copper foil for fast growth of large single-crystal graphene under free molecular flow. *Adv. Mater.*, in press, DOI: 10.1002/adma.201603579.
- [32] Vlassiouk, I.; Regmi, M.; Fulvio, P. F.; Dai, S.; Datskos, P.; Eres, G.; Smirnov, S. Role of hydrogen in chemical vapor deposition growth of large single-crystal graphene. *Acs Nano* 2011, 5, 6069–6076.
- [33] Ma, T.; Ren, W. C.; Liu, Z. B.; Huang, L.; Ma, L.-P.; Ma, X. L.; Zhang, Z. Y.; Peng, L.-M.; Cheng, H.-M. Repeated growth–etching–regrowth for large-area defect-free single-crystal graphene by chemical vapor deposition. *Acs Nano* 2014, 8, 12806–12813.
- [34] Whiteway, E.; Yang, W.; Yu, V.; Hilke, M. Time evolution of the growth of single graphene crystals and high resolution isotope labeling. 2015, arXiv:1509.01579. arXiv.org e-Print archive. http://arxiv.org/abs/1509.01579 (accessed Jul 27, 2015).
- [35] Lin, L.; Sun, L. Z.; Zhang, J. C.; Sun, J. Y.; Koh, A. L.; Peng, H. L.; Liu, Z. F. Rapid growth of large single-crystalline graphene via second passivation and multistage carbon supply. *Adv. Mater.* **2016**, *28*, 4671–4677.
- [36] Wang, S. N.; Suzuki, S.; Hibino, H. Raman spectroscopic investigation of polycrystalline structures of CVD-grown graphene by isotope labeling. *Nanoscale* 2014, 6, 13838– 13844.